Identification of Drug-Like Inhibitors of Insulin-Regulated Aminopeptidase Through Small-Molecule Screening

Karin Engen,[1] Ulrika Rosenström,[1] Hanna Axelsson,[2] Vivek Konda,[1] Leif Dahllund,[3] Magdalena Otrocka,[2] Kristmundur Sigmundsson,[2,] Alexandros Nikolaou,[4,†] Georges Vauquelin,[4] Mathias Hallberg,[5] Annika Jenmalm Jensen,[2] Thomas Lundbäck,[2] and Mats Larhed[6]*

[1]Division of Organic Pharmaceutical Chemistry, Department of Medicinal Chemistry, Uppsala University, Uppsala, Sweden.
[2]Chemical Biology Consortium Sweden, Science for Life Laboratory Stockholm, Division of Translational Medicine and Chemical Biology, Department of Medical Biochemistry and Biophysics, Karolinska Institutet, Solna, Sweden.
[3]Drug Discovery and Development Platform, Science for Life Laboratory Stockholm, Solna, Sweden.
[4]Department of Molecular and Biochemical Pharmacology, Vrije Universiteit Brussel, Brussels, Belgium.
[5]Beijer Laboratory, Division of Biological Research on Drug Dependence, Department of Pharmaceutical Biosciences, Uppsala University, Uppsala, Sweden.
[6]Science for Life Laboratory Uppsala, Division of Organic Pharmaceutical Chemistry, Department of Medicinal Chemistry, Uppsala University, Uppsala, Sweden.
**Present address: Program of Cardiovascular and Metabolic Disorders, Duke-NUS Medical School, Singapore, Singapore.*
[†]Present address: Centre for Genomic Regulation, Barcelona, Spain.

ABSTRACT

Intracerebroventricular injection of angiotensin IV, a ligand of insulin-regulated aminopeptidase (IRAP), has been shown to improve cognitive functions in several animal models. Consequently, IRAP is considered a potential target for treatment of cognitive disorders. To identify nonpeptidic IRAP inhibitors, we adapted an established enzymatic assay based on membrane preparations from Chinese hamster ovary cells and a synthetic peptide-like substrate for high-throughput screening purposes. The 384-well microplate-based absorbance assay was used to screen a diverse set of 10,500 compounds for their inhibitory capacity of IRAP. The assay performance was robust with Z′-values ranging from 0.81 to 0.91, and the screen resulted in 23 compounds that displayed greater than 60% inhibition at a compound concentration of 10 μM. After hit confirmation experiments, purity analysis, and promiscuity investigations, three structurally different compounds were considered particularly interesting as starting points for the development of small-molecule-based IRAP inhibitors. After resynthesis, all three compounds confirmed low μM activity and were shown to be rapidly reversible. Additional characterization included activity in a fluorescence-based orthogonal assay and in the presence of a nonionic detergent and a reducing agent, respectively. Importantly, the characterized compounds also showed inhibition of the human ortholog, prompting our further interest in these novel IRAP inhibitors.

INTRODUCTION

More than 46 million people worldwide suffer from cognitive impairment or age-related cognitive decline, and this number is estimated to increase to more than 130 million by 2050.[1] Consequently, there is a strong and urgent demand to develop new treatment approaches for these disorders. A prerequisite for such activities is the identification of well-validated mechanisms and the chemical entities required to test these in suitable preclinical models of cognition. Our lab has a longstanding interest in the hexapeptide angiotensin IV (Ang IV), a degradation fragment of angiotensin II, as intracerebroventricular injections were shown to improve memory and learning in a large variety of animal models.[2–8]

High densities of binding sites for Ang IV are observed in regions of the brain associated with sensory, motor, and cognitive functions, for example, the hippocampus.[3,9–12] At the time of the discovery, these sites of binding were referred to as the AT4 receptor, although the nature of this receptor was largely unknown. In 2001, the AT4 receptor was identified as the insulin-regulated aminopeptidase (IRAP), a single-spanning transmembrane zinc-metallopeptidase that belongs to the M1 family of aminopeptidases, and on which Ang IV acts as an inhibitor of the catalytic activity.[13] IRAP is known to play multiple functional roles, including the processing of cyclic peptides such as oxytocin and vasopressin,[14,15] the trimming of MHC peptides,[16] and the colocalization with

DOI: 10.1089/adt.2016.708

Glut4 when the latter translocates to the cell membrane on insulin stimulation.[17]

Given the potential importance of IRAP in cognitive disorders, several efforts have been undertaken to develop modulators of its enzymatic activity. The Vauquelin group focused on peptide-based inhibitors containing β-homo amino acids and constrained amino-acid analogs of Ang IV with inhibitory constants (K_i's) in the low nM range.[18–20] Our group has utilized Ang IV and the IRAP substrate oxytocin, the latter encompassing a macrocyclic disulfide at the cleavage site, as starting points in the development of IRAP inhibitors. Truncated analogs of Ang IV, and *N*-terminal cyclizations thereof, provided highly potent macrocyclic IRAP inhibitors with K_i's down to 1.8 nM.[21–25] Although this set of peptidomimetic structures was found to be metabolically relatively stable and could enhance dendritic spine density in rat hippocampal primary cultures,[26] they suffer from poor permeability and hence are of limited use as *in vivo* pharmacological tools to further study the role of IRAP inhibition in models of cognition. The Stratikos group have utilized transition state mimicking compounds based on a zinc-chelating phosphinic group, and representatives of these compounds show excellent activity ($IC_{50} = 30$ nM), but poor selectivity toward the closely related endoplasmic reticulum aminopeptidase (ERAP) 1 and 2.[27] A similar approach using a 3,4-diaminobenzoic acid as a scaffold led to pseudopeptides with good potency as well as to an improved selectivity profile toward ERAP1 and ERAP2.[28,29]

In parallel, the first drug-like nonpeptidic IRAP inhibitors were identified and optimized by using a virtual screening approach.[30,31] *In vivo* efficacy was demonstrated in rodent models of cognition for one of these inhibitors, a pyridine-substituted benzopyran scaffold. The performance in both spatial working and recognition memory paradigms was improved after administration into the lateral ventricles. However, the compound suffered from short elimination half-life and high plasma clearance.[31]

Since most of the available IRAP inhibitors are still peptide based, suffering from inadequate selectivity and/or poor permeability, we initiated a collaborative effort to identify less complex small-molecule-based inhibitors of IRAP. An existing enzymatic assay was used as a starting point for the development of a screen compatible assay that was adapted to 384-well microtiter plate format and automated liquid handling procedures. We hereby report on the development of the assay, the outcome of the screening of $\sim$10,500 lead-like and drug-like compounds, and the subsequent hit confirmation experiments in which the structure, the chemical stability, the concentration dependency, and the reversibility of the identified inhibitors were confirmed. The study resulted in the identification of three novel chemical clusters of IRAP inhibitors, with the most potent representatives in the low μM range.

MATERIALS AND METHODS

Cell Culture Conditions

Chinese hamster ovary (CHO) cells were cultured in 75 cm^2 cell culture flasks (430641U; Corning) or Nunc™ EasyFill™ Cell Factory™ System 2528 cm^2 (140360; Nunc) in Dulbecco's modified essential medium (D6046; Sigma-Aldrich) that was supplemented with 2 mM L-glutamine (D7513; Sigma-Aldrich), 100 IU/mL penicillin and 0.1 mg/mL streptomycin (P4333; Sigma-Aldrich), 1% (v/v) nonessential amino-acids (M7145; Sigma-Aldrich), 1 mM sodium pyruvate (S8636; Sigma-Aldrich), and 10% (v/v) heat-inactivated fetal bovine serum (F9665; Sigma-Aldrich). The cells were grown in a humidified cell incubator at 37°C and 5% CO_2 until the cells were about 90% confluent. Before harvesting, the cells were washed with phosphate-buffered saline (PBS, D8537; Sigma-Aldrich) and then treated for 5 min at 37°C with Versene (BE17-711E; Lonza). The detached cells were suspended in PBS and centrifuged for 5 min at $500 \times g$ at room temperature. The resulting cell pellet was resuspended in PBS, the cells were counted before they were centrifuged again, and the cell pellets were stored at −20°C until they were used.

Overexpression of Human IRAP

Overexpression of human IRAP was achieved in Freestyle HEK293-F Cells (R790-07; Invitrogen) that were grown in 80 mL of Freestyle Expression Medium (12338-018; Invitrogen). The cell culture was grown in 250 mL Erlenmeyer flasks (431144.40; Corning) that were kept at 37°C, 8% CO_2, and 70% relative humidity and with shaking at 130–135 rpm in an Infors Multitron incubator. The cells were transfected with 1.1 μg plasmid/10^6 cells (pCIneo containing the gene of human IRAP, obtained from Prof. M. Tsujimoto, Laboratory of Cellular Biochemistry, Saitama, Japan) in the presence of 2 μg polyethyleneimine/10^6 cells (Polyethyleneimine, linear, MW-25 000, Cat. No. 23966; Polysciences). Before the overexpression studies, the plasmid was transfected and propagated in Mach1 *Escherichia coli* (C8620-03; Invitrogen), from where the plasmid DNA was prepared by using QIAGEN Plasmid Plus Maxi Kit (12963). Forty-eight hours post-transfection, the cells were harvested by centrifugation at $130 \times g$ for 3 min. The cells were washed once with PBS, and the cell pellets were stored at −20°C until they were used for membrane preparations.

Membrane Preparation

All experiments were based on membrane preparations from either CHO cells or HEK293T suspension cells overexpressing human IRAP. Membrane preparation was achieved essentially as previously described[32] by using the following procedure. Washed cell pellets were taken out of the −20°C freezers, quickly thawed, and placed on ice. Pellets were resuspended in ice-cold 50 mM Tris-HCl at pH 7.4 that was supplemented with 0.1 mM of phenylmethanesulfonyl fluoride (PMSF, 78830; Sigma-Aldrich) and were then sonicated for 3 × 15 s with 30 s interruption time by using a Branson Digital sonifier 250. The sonicated cells were then transferred to a Dounce homogenizer and were homogenized by a minimum of 20 strokes while keeping everything on ice. The homogenate was thereafter transferred to ice-cold tubes and centrifuged at 4°C and 30,000× *g* for 30 min. The supernatant was discarded; the membranes were resuspended in buffer, again homogenized by using the Dounce homogenizer (20 strokes), and centrifuged as described earlier. This procedure was repeated twice, and the final membrane pellet was then kept frozen at −20°C until it was used.

Compound Library Storage and Handling

A set of 10,500 compounds from the primary screening set at Chemical Biology Consortium Sweden (CBCS) was applied in this screening campaign. A majority of the compound library was donated by former Biovitrum AB and is a mix of commercially available and proprietary compounds. Compound stock solutions at 10 mM in dimethyl sulfoxide (DMSO) were stored and frozen at −20°C under low humidity conditions in individual capped tubes in REMP 96 Storage Tube Racks located in REMP Small-Size Store™. DMSO stock solutions for follow-up studies are retrieved directly from the REMP vials by cherry-picking. For screening purposes, the compound solutions were transferred to Labcyte 384 LDV plates (LP-0200) and then further into Labcyte 1536 HighBase plates (LP-03730) to enable dispensing by using acoustic liquid handling equipment. The compound solutions (75 nl) were dispensed directly into columns 1–22 of the assay plates (242757; Nunc) by using an Echo 555™ acoustic liquid handler (LabCyte). The Echo was also used to dispense the equivalent volume of DMSO (negative control, 0% inhibition), and a 10 mM DMSO solution of AL-11[19,33] (positive control, 100% inhibition), in columns 23 and 24, with DMSO in rows A–H and AL-11 in rows I–P. The final compound concentration used in the screen was 10 μM, with a final DMSO concentration of 0.1% in all wells.

Screening Campaign

Small-molecule library screening was accomplished in transparent 384-well plates with preplated compound solutions and controls in all wells (75 nl). A homogenized solution of IRAP-containing CHO cell membranes was prepared on ice by using a minimal of 20 strokes in a Dounce homogenizer in an ice-cold solution of 50 mM Tris-HCl, 150 mM NaCl, and 0.1 mM PMSF at pH 7.4. This solution was kept on ice until 25 μL thereof was added to each well of the assay plates by using a MultiDrop Combi (Thermo Scientific), resulting in membranes from 25,000 cells in each well. This was followed by the addition of 50 μL of a substrate solution containing 1.5 mM L-leucine-*para*-nitroanilide (L-Leu-*p*-NA, L9125; Sigma-Aldrich), which was prepared by diluting a 100 mM stock solution in 2-methoxyethanol into the same assay buffer. Thus, the final substrate concentration in the assay was 1 mM. A first reading was taken immediately on an Envision (PerkinElmer) with the monochromator set at 405 nm to get a background reading (which allows for background corrections for colored compounds). The plates were then kept dark and incubated at room temperature, with new readings taken after 8, 17, and 25 h to ensure data were collected at various time points of the enzymatic reaction.

IRAP Activity Assay for Concentration-Response Characterizations in 96-Well Format

Concentration-response experiments measuring the impact of identified inhibitors on IRAP activity as a function of compound concentration were conducted in several different formats. The absorbance assay, based on the L-Leu-*p*-NA substrate, was performed in transparent 96-well plates (269620; Nunc) in a final assay volume of 200 μL per well. Compound stock solutions (10 mM in DMSO) were serially diluted in DMSO by a factor of 1/2 in columns 1–11 of round-bottomed polypropylene plates (267245; Nunc). Column 12 was reserved for controls with the equivalent amount of DMSO added to wells A12-D12 (negative control, 0% inhibition), whereas a 1 mM stock solution of IVDE77[20] in DMSO was added to wells E12-H12 (positive control, 100% inhibition). The DMSO solutions were then diluted in assay buffer (same as for the screen) and transferred to triplicate assay plates (50 μL to each well). A dilute solution of homogenized CHO cell membranes (50 μL) and substrate (100 μL) were then added to initiate the enzymatic reaction. This gave a final presence of 1 mM L-Leu-*p*-NA and CHO cell membranes from 50,000 to 250,000 cells (varies between experiments) per well. The plates were heat sealed, kept dark, and incubated at room temperature until a statistically significant difference between the controls was observed (~8–17 h). Intermittent measurements were taken to ensure the readings were taken under conditions of near-linear progression (<50% substrate conversion). Concentration-response experiments using the human

ortholog of IRAP were conducted by using the identical setup as for the absorbance-based CHO cell membrane assay. Aliquots of membranes from HEK293 suspension cells overexpressing IRAP were thawed, suspended in assay buffer, homogenized using the Dounce homogenizer, and diluted with assay buffer.

Concentration-response experiments based on solubilized enzyme were conducted by using the same setup, except for the treatment of the CHO cell membranes before addition to the plates and the presence of Triton X-100 in the assay buffer. For these experiments, aliquots of membranes were thawed, suspended in assay buffer, and homogenized by using the Dounce homogenizer (20 strokes). Triton X-100 was then added to give a final presence of 1% in the membrane containing buffer, and the suspension was subsequently rotated for at least 5 h at 4°C to solubilize the membrane proteins. After solubilization, membranes were pelleted by centrifugation at 10,000× *g* in a tabletop centrifuge at 4°C for 15 min. The supernatant was used as the source of IRAP activity and was applied at a volume of 50 μL per well. This procedure gave a final IRAP concentration corresponding to the content of 322,000 cells per well. Concentration-response experiments for controlling redox reactivity of the hits were conducted by using the standard absorbance-based assay with CHO cell membranes, but with the addition of dithiothreitol (DTT) to a final concentration of 1 mM in the assay buffer.

Concentration-response experiments in an orthogonal assay utilizing a fluorescence-based readout were performed in black, low-volume 96-well plates (3686; Corning). The experimental design was identical to what is described earlier, except for the substrate and the order of addition to the assay plates. Here, the substrate solution was 150 μM L-Leucine-7-amido-4-methylcoumarin (L-Leu-AMC, L2145; Sigma-Aldrich), which was prepared by diluting a 62 mM stock solution of the substrate in DMSO into the assay buffer. The diluted compound solutions and controls were transferred to the assay plates in triplicate (20 μL per well), followed by substrate solution (20 μL) and diluted homogenized CHO cell membranes (40 μL). The assay was conducted with a final concentration of 37.5 μM L-Leu-AMC and CHO cell membranes from 130,000 cells per well. Fluorescence readings were taken on a Victor3 multiplate reader (PerkinElmer) by using an excitation filter at 355 nm and an emission filter at 460 nm.

Data Analysis

Raw data from the microplate readers were imported into Microsoft Excel and GraphPad Prism 6 for analysis and visualization. Determination of Z′-factor values were done based on the controls of each plate as described.[34] All data were converted into % inhibition values based on the negative (0%) and positive (100%) controls on each plate. Data from triplicate samples were averaged, and the curves were fitted to a four-parameter concentration-response model within IDBS XLfit (model 205) or GraphPad Prism 6 to obtain best-fit values for the IC_{50}, Hill slope, and the upper and lower limits of the concentration-response curve.

Measurements of Identity and Purity of Test Compound Solutions

Assessment of identity and purity of the test solutions that were used for hit confirmation purposes, that is, those being stored in REMP vials, was done by means of reversed-phase high-performance liquid chromatography coupled to mass spectrometry (HPLC-MS). A small aliquot of each test solution (2 μL of a 10 mM solution) was placed in a deep-well plate and was diluted with 20 μL of methanol. The plate was then placed in an Agilent 1100 HPLC UV/MS with electrospray ionization (ESI+). The HPLC method was based on an ACE C8 3 μm column (3.0 × 50 mm) and a mobile phase [0.1% CF_3COOH/CH_3CN]/[0.1% CF_3COOH/H_2O]. All solvents were HPLC grade, and absorbance was monitored at 305 ± 90 and 254 nm. Compounds that did not give satisfactory data were re-analyzed by using a method based on a Waters XBridge C18 3.5 μm column (3.0 × 50 mm), 3.5 min gradient mobile phase [CH_3CN]/[10 mM NH_4HCO_3/H_2O]. The instrument software was used to integrate the UV response for each peak and provided a list of the peaks and their associated masses. The estimated purity was calculated based on the integrated area for the expected mass compared with the areas of all other peaks. The result was manually controlled and if there were deviations from the expected outcome, a meticulous investigation of the UV response and mass spectrometry was performed.

Hit Resynthesis and Characterization

General information and materials. All chemicals were purchased from Sigma-Aldrich and were used as received. Purification was performed by flash column chromatography using silica gel (60–120 mesh size) and for test compounds also, reversed-phase HPLC (UV-triggered, 254 nm) fraction collection was done with a Gilson Trilution HPLC system, using a Macherey-Nagel Nucleodur C18 column (21 × 125 mm, 5 μm particle size), and H_2O/CH_3CN/0.1% CF_3COOH as eluent in a gradient (30%–70%, 10 mL min^{-1} over 15 min). Analytical HPLC-MS spectrometry was performed on a Dionex UltiMate 3000 HPLC system with a Thermo Scientific MSQ Plus mass spectrometer (ESI+) and detection by UV (diode array detector), using a Phenomenex Kinetex C18 column (50 × 30 mm, 2.6 μm particle size, 100 Å pore size). A gradient of H_2O/CH_3CN/0.1% HCOOH at a flow rate of 1.5 mL min^{-1} was used. High-resolution

mass spectra (HRMS) were recorded on a Micromass Q-Tof2 mass spectrometer that was equipped with an electrospray ion source. ^{1}H and ^{13}C NMR spectra were recorded at 25°C on a Varian 400-MR spectrometer at 400 and 100 MHz, respectively. For rotamers, NMR experiments were performed both at room temperature and at elevated temperature; see Supplementary Data (Supplementary Data are available online at www.liebertpub.com/adt). Chemical shifts are reported in ppm, with the solvent residual peak as the internal standard ($CDCl_3$ δ_H 7.26, δ_C 77.16; CD_3OD δ_H 3.31, δ_C 49.00; DMSO-d_6 δ_H 2.50, δ_C 39.52). The synthesis and characterization of compounds **2**[35] and **7**[36] have been previously reported.

(2-Methoxyphenyl)(pyridine-2-yl)methanamine (24). A solution of 2-cyanopyridine (0.5 mL, 5.2 mmol) in dry toluene (25 mL) under inert atmosphere was cooled to 0°C on an ice bath. Then, 2-Methoxymagnesiumbromide in THF (1 M, 6.2 mL, 6.2 mmol) was added dropwise. The reaction mixture was stirred for 40 min at 0°C. Isobutanol was added dropwise to a clear brown solution. $NaBH_4$ (393 mg, 10.4 mmol) was added, and the mixture was stirred at ambient temperature for 14 h. The reaction was quenched with a 1:1 mixture of MeOH and H_2O, and the organic solvents were removed under reduced pressure. The remaining aqueous mixture was extracted with DCM (×3) and the combined organic phases were washed with brine, dried over $MgSO_4$, filtered, and concentrated. The crude product was purified by flash column chromatography by using 5% MeOH in $CHCl_3$ as eluent to afford **24** as a yellow oil (1.06 g, 95%): ^{1}H NMR (400 MHz, CD_3OD) δ 8.48 (ddd, J = 1.0, 1.9, 5.0 Hz, 1H), 7.72 (td, J = 1.8, 7.7 Hz, 1H), 7.35 (dt, J = 1.0, 7.6 Hz, 1H), 7.27–7.21 (m, 3H), 6.98–6.90 (m, 2H), 5.45 (s, 1H), 4.85 (s, 2H), and 3.78 (s, 3H); ^{13}C NMR (101 MHz, $CDCl_3$) δ 163.4, 156.8, 149.1, 136.3, 133.3, 128.2, 127.8, 121.8, 121.7, 120.9, 110.7, 55.4, and 55.0.

(2S)-tert-Butyl-2-(((2-methoxyphenyl)(pyridine-2-yl)methyl)-carbamoyl)pyrrolidine-1-carboxylate (25). To a solution of **24** (300 mg, 1.4 mmol), *N*-Boc-L-Proline (362 mg, 1.7 mmol), HOBt (257 mg, 1.7 mmol), and TEA (0.4 mL, 2.9 mmol) in dry DCM (14 mL) were added to EDC*HCl (322 mg, 1.7 mmol). The reaction mixture was stirred at room temperature for 3 h, washed with H_2O and brine, dried over $MgSO_4$, filtered, and concentrated under reduced pressure. The crude product was purified by flash column chromatography by using 3% MeOH in $CHCl_3$ as eluent to afford **25** as a white semi-solid, mixture of diastereomers (1:1) and rotamers (542 mg, 94%): $[\alpha]_D^{22}$-68° (c = 1.12, $CHCl_3$); ^{1}H NMR (400 MHz, DMSO-d_6) δ 8.59 (d, J = 8.3 Hz, 1H, 1 isomer) 8.52 (d, J = 8.3 Hz, 1H, 1 isomer), 8.49–8.44 (m, 1H+1H, 2 isomers), 7.77–7.68 (m, 1H+1H, 2 isomers), 7.47–7.18 (m, 4H+4H, 2 isomers), 6.98 (dd, J = 2.2, 1.1 Hz, 1H, 1 isomer), 6.95 (dd, J = 2.2, 1.1 Hz, 1H, 1 isomer), 6.94–6.86 (m, 1H+1H, 2 isomers), 6.45 (t, J = 8.9 Hz, 1H, 1 isomer), 6.37 (t, J = 7.2 Hz, 1H, 1 isomer), 4.35–4.21 (m, 1H+1H, 2 isomers), 3.75 (d, J = 2.3 Hz, 3H+3H, 2 isomers), 3.34 (m, 3H+3H, 2 isomers), 2.19–1.96 (m, 1H+1H, 2 isomers), 1.90–1.68 (m, 3H+3H, 2 isomers), and 1.47–1.16 (m, 9H+9H, 2 isomers); and ^{13}C NMR (101 MHz, DMSO-d_6) δ *Isomer 1:* 171.51 (major rotamer), 171.1 (minor rotamer), 160.6, 156.3, 153.8, 148.8, 136.64, 129.7, 128.4, 128.2, 122.13, 121.8 (major rotamer), 121.6 (minor rotamer), 120.2, 111.0, 78.8 (minor rotamer), 78.42 (major rotamer), 59.6 (major rotamer), 59.4 (minor rotamer), 55.43, 51.9, 46.7, 31.0, 28.1, and 23.9. *Isomer 2:* 171.46 (major rotamer), 171.0 (minor rotamer), 160.2, 156.3, 153.4, 148.8, 136.55, 129.5, 128.3, 127.5, 122.08, 121.42 (minor rotamer), 121.25 (major rotamer), 120.2, 111.0, 78.7 (minor rotamer), 121.36 (major rotamer), 120.2, 110.94, 78.71 (minor rotamer), 78.36 (major rotamer), 59.5 (major rotamer), 59.3 (minor rotamer), 55.40, 51.7, 46.5, 29.5, 27.8, and 23.1.

(S)-tert-Butyl-2-(1-(2-methoxyphenyl)imidazo[1,5-α]pyridine-3-yl)pyrrolidine-1-carboxylate (26). A solution of **25** (300 mg, 0.73 mmol) and pyridine (0.35 mL, 4.37 mmol) in dry DCM (5 mL) under inert atmosphere was cooled to 0°C on an ice bath, and $POCl_3$ (0.12 mL, 1.3 mmol) was added dropwise. The reaction mixture was stirred at room temperature for 14 h. The reaction mixture was washed with NaOH (1%, aq), dried over $MgSO_4$, filtered, and concentrated under reduced pressure. The crude product was purified by flash column chromatography by using 30% EtOAc in pentane as eluent to afford **26** as a brown oil (240 mg, 84%): ^{1}H NMR (400 MHz, DMSO-d_6, 100°C) δ 8.26 (d, J = 7.2 Hz, 1H), 7.60 (dd, J = 7.6, 1.8 Hz, 1H), 7.47 (dt, J = 9.2, 1.3 Hz, 1H), 7.29 (ddd, J = 8.3, 7.3, 1.8 Hz, 1H), 7.10 (dd, J = 8.2, 1.1 Hz, 1H), 7.02 (td, J = 7.4, 1.1 Hz, 1H), 6.73 (ddd, J = 9.2, 6.3, 1.0 Hz, 1H), 6.64 (ddd, J = 7.4, 6.3, 1.3 Hz, 1H), 5.35 (dd, J = 7.4, 4.6 Hz, 1H), 3.80 (s, 3H), 3.62–3.49 (m, 2H), 2.38–2.21 (m, 2H), 2.19–2.11 (m, 1H), and 2.01–1.90 (m, 1H), 1.18 (s, 9H); ^{13}C NMR (101 MHz, DMSO-d_6, 100°C) δ 156.7, 154.1, 140.0, 131.4, 131.2, 127.4, 127.2, 125.0, 122.4, 120.4, 120.1, 118.2, 112.3, 78.9, 56.1, 55.9, 53.1, 46.9, 28.5, 28.3, and 24.1.

(S)-1-(2-Methoxyphenyl)-3-(pyrrolidine-2-yl)imidazo[1,5-α]pyridine hydrochloride (27). To a solution of **26** (230 mg, 0.59 mmol) in dioxane, HCl in dioxane (4M, 1.5 mL, 5.9 mmol) was added and the reaction mixture was stirred overnight. The obtained beige salt **27** was filtered and used in the next step without further purification (170 mg, 99%, >99% pure according to LCMS): $[\alpha]_D^{23}$-7.1° (c = 1.10, MeOH); ^{1}H NMR (400 MHz, CD_3OD) δ 8.19 (dt, J = 7.2, 1.1 Hz, 1H), 7.53 (ddd, J = 7.5, 1.8,

0.4 Hz, 1H), 7.42 (dt, J=9.3, 1.2 Hz, 1H), 7.34 (ddd, J=8.3, 7.4, 1.8 Hz, 1H), 7.10 (dd, J=8.3, 1.1 Hz, 1H), 7.04 (td, J=7.4, 1.1 Hz, 1H), 6.77 (ddd, J=9.3, 6.4, 1.0 Hz, 1H), 6.69 (ddd, J=7.2, 6.4, 1.3 Hz, 1H), 4.64 (t, J=7.6 Hz, 1H), 3.81 (s, 3H), 3.22–3.14 (m, 1H), 2.02–3.94 (m, 1H), 2.35–2.21 (m, 2H), 2.11–2.00 (m, 1H), and 1.99–1.88 (m, 1H); and ^{13}C NMR (101 MHz, CD_3OD) δ 158.1, 140.1, 132.4, 129.8, 129.6, 128.1, 124.7, 122.7, 121.7, 121.1, 119.8, 114.0, 112.5, 55.9, 55.3, 47.7, 31.4, and 27.0.

(S)-2-(1-(2-Methoxyphenyl)imidazo[1,5-a]pyridin-3-yl)-N-((S)-1-phenylethyl)pyrrolidine-1-carboxamide. To a solution of **27** (60 mg, 0.18 mmol) and TEA (76 µL, 0.55 mmol) in dry MeCN (1.8 mL) under inert atmosphere, (*S*)-(-)-α-methylbenzyl isocyanate (51 µL, 0.36 mmol) was added and the mixture was stirred at room temperature for 20 min. The reaction mixture was concentrated under reduced pressure, and the crude products were purified by flash column chromatography (2% MeOH in $CHCl_3$) followed by preparative HPLC to afford compound **5** as white solid (57 mg, 71%): $[\alpha]_D^{24}$-34° (c=0.54, $CHCl_3$); ^{1}H NMR (400 MHz, DMSO-d_6, rotamers) δ 8.54 (d, J=7.3, 1H), 7.63–7.37 (m, 3H), 7.32–6.97 (m, 9H), 6.82 (t, J=6.9 Hz, 1H), 5.59 (dd, J=7.8, 4.1 Hz, 1H), 4.75 (q, J=7.2 Hz, 1H), 3.80 (s, 3H), 3.73–3.67 (m, 1H), 3.53–3.45 (m, 1H), 2.40–2.29 (m, 1H), 2.19–2.08 (m, 2H), 2.08–1.97 (m, 1H), and 1.34 (d, J=7.1 Hz, 3H); ^{13}C NMR (101 MHz, DMSO-d_6, rotamers) δ 158.4, 158.0, 156.4, 156.3, 155.8, 155.7, 146.0, 145.5, 138.9, 138.9, 131.3, 131.2, 128.1, 128.0, 126.4, 126.4, 126.3, 126.3, 125.92, 125.91, 122.9, 122.8, 120.72, 120.68, 119.5, 119.4, 111.9, 55.6, 55.5, 52.2, 52.0, 49.3, 49.1, 46.2, 30.83, 30.77, 24.60, 24.56, 22.9, and 22.8; and HRMS (ESI+): m/z $[M + H]^+$ calcd for $C_{27}H_{29}N_4O_2$: 441.2291, found: 441.2289.

RESULTS

Assay Adaptation to a 384-Well Microplate Format

The enzymatic activity of IRAP can be studied by several different means, including HPLC analysis of the aminopeptidase activity toward endogenous substrates as well as the use of synthetic substrates for which the absorbance (L-Leu-*p*-NA) or fluorescence (L-Leu-AMC) is altered on peptide bond cleavage.[37,38] For screening purposes, we wished to adopt an assay design that is compatible with a 384-well microtiter plate format and the use of membrane preparations such that IRAP is still attached to the membranes. Our choice fell on the L-Leu-*p*-NA substrate given its simplicity and our extensive experience with its use for inhibitor characterization. Given that the product of this substrate absorbs light at wavelengths that are close to the near-UV range (405 nm), we were initially concerned with potential interference from colored compounds in the compound library. We also considered a commonly used coumarin-based fluorogenic substrate, but as this is excited at even shorter wavelengths it was instead used for counterscreening (see below). In an effort to compensate for

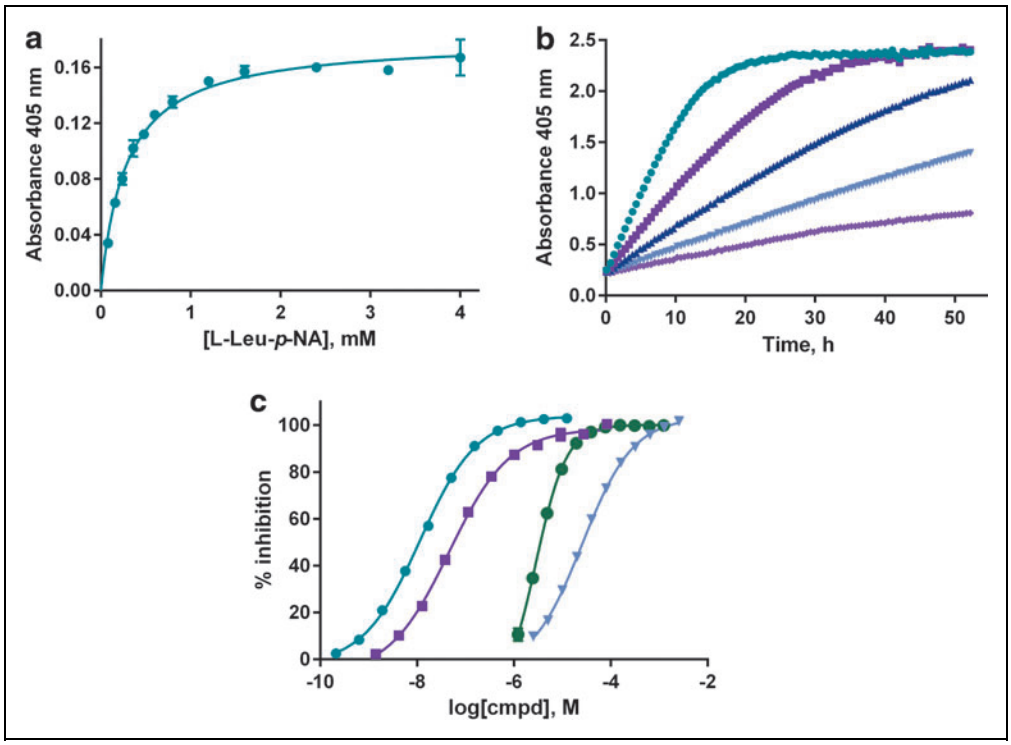

Fig. 1. Assay characterization in the 384-well microtiter plate format. **(a)** Apparent IRAP activity in CHO cell membrane preparations as a function of L-Leu-*p*-NA concentration (*teal* ●). Data are shown as the average and standard deviation of measurements done in triplicate. The *solid line* represents the best fit to the Michaeli-Menten model within GraphPad Prism, resulting in an apparent K_m value of 0.28±0.02 mM. **(b)** Time-course experiment for the IRAP activity as a function of membrane concentration at a substrate (L-Leu-*p*-NA) concentration of 1 mM; membranes from 90,000 (*teal* ●), 45,000 (■), 22,500 (▲), 11,250 (▼), or 5,625 (◆) CHO cells per well. **(c)** Pharmacological response of the IRAP assay based on CHO cell membranes and 1 mM L-Leu-*p*-NA to known inhibitors; IVDE77 (*teal* ●), AL-11 (■), $ZnCl_2$ (*green* ●), and Amastatin (▼). Data are shown as the average and standard deviations from measurements done in triplicate. The solid lines represent best fits to a four-parameter sigmoidal curve in GraphPad Prism. CHO, Chinese hamster ovary; IRAP, insulin-regulated aminopeptidase. Color images available online at www.liebertpub.com/adt

the presence of colored library compounds, the screen was run in semi-kinetic mode, with readings taken at several time points. As discussed later, these worries were largely unwarranted. As a source of enzyme activity, we opted for wild-type CHO cell membranes, as these are known to be an abundant source of endogenous IRAP activity, with minimal contamination from other aminopeptidases and with significant activity toward this substrate.[32,39]

A number of changes had to be made to our standard assay format to facilitate the screening logistics. The most significant of these involved a change from 37°C to room temperature incubation to avoid plate edge effects,[40] prolonged incubation times to use less membranes on a per-well basis, and the use of automated liquid handling for compound, membrane, and substrate dispenses. After substrate K_m determinations and membrane titrations in the form of time-course experiments to ensure less than 50% substrate conversion (*Fig. 1a, b*), we used known peptidic and small-molecule-based inhibitors to investigate whether the assay was responding pharmacologically as expected. The assay accurately ranked the metabolically stable peptidic-based inhibitors IVDE77[20] and AL-11,[19] with IC_{50} values of 11 and 55 nM, respectively, as well as the high μM inhibitor amastatin (*Fig. 1c*). We also confirmed the low μM inhibitory activity of $ZnCl_2$ as previously reported.[37]

Table 1. Protocol for the IRAP Inhibition Assay

Step	Parameter	Value	Description
1	Add controls	75 nl	10 mM AL-11 (positive) or DMSO (negative)
2	Add compounds	75 nl	10 mM in DMSO
3	Add enzyme	25 μL	Homogenized IRAP CHO cell membranes
4	Add substrate	50 μL	1.5 mM L-Leu-*p*-NA in assay buffer
5	Incubate	17 h	Room temperature
6	Assay readout	405 nm	Envision plate reader

Step Notes

1. Transparent 384-well plate, Nunc no. 242757. Echo 555™ acoustic liquid handler. Controls were added to columns 23 and 24 of the assay plates.
2. Echo 555 acoustic liquid handler. One thousand-fold assay concentration.
3. MultiDrop Combi instrument. Prepared by diluting the CHO cell membranes to 500 mL in ice-cold buffer (988,000 cells/mL). The assay buffer consists of 50 mM Tris-HCl, 150 mM NaCl, and 0.1 mM PMSF at pH 7.4. Final amount of 25,000 cells/well.
4. MultiDrop Combi Instrument. Prepared by diluting a 100 mM stock solution in 2-methoxythanol into the assay buffer. Final assay concentration is 1 mM.
5. Plates lidded and kept dark.
6. Absorbance measured.

CHO, Chinese hamster ovary; DMSO, dimethyl sulfoxide; IRAP, insulin-regulated aminopeptidase; L-Leu-*p*-NA, L-leucine-*para*-nitroanilide; PMSF, phenylmethanesulfonyl fluoride.

Library Screening and Hit Confirmation

Using the microtiter plate formatted assay for IRAP, we completed a screening campaign by using the primary screening set at CBCS (www.cbcs.se). A protocol with details on the screen logistics is provided in *Table 1*.

The increase in absorbance over time as the synthetic substrate was processed by IRAP was followed at four different time points, including a control reading immediately after the initiation of the reaction. This first reading allowed a compensation of any absorbance contributed by colored compounds in the library. However, contrary to our fears of

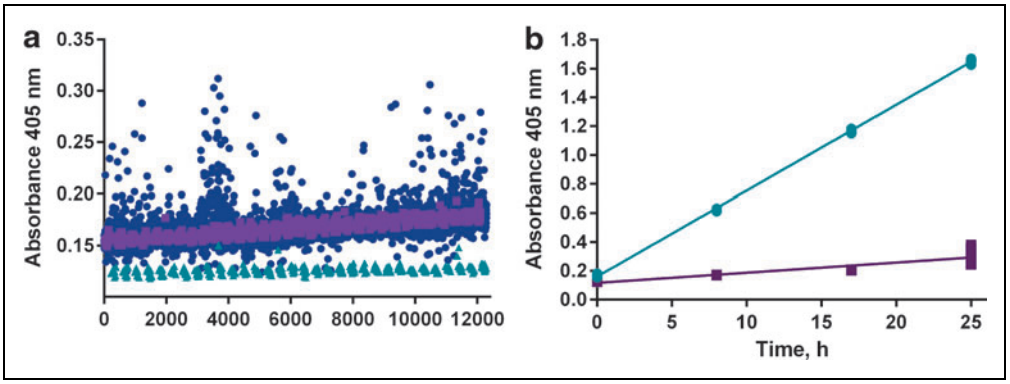

Fig. 2. Investigation of compound interference and linearity of reaction under screen conditions. **(a)** Absorbance readings for all library compounds at a concentration of 10 μM shortly after addition of the substrate solution (*dark blue* ●), that is, at an incubation time close to 0 h. The corresponding absorbance readings are also shown for the DMSO controls (■) and the fully inhibited controls in the presence of 10 μM of AL-11 (▲). The *x*-axis represents the number of data points, with sequential readings from well A1 through to P24 in the 384-well plates (32 included in the screen). **(b)** Absorbance readings for the controls located in columns 23 and 24 in the screening plates with readings taken at four different time points, that is, shortly after addition of substrates ($t = 0$ h) and after 8, 17, and 25 h of incubation, respectively. Each symbol is given as the average and standard deviation of 16 controls each on the 32 screening plates with DMSO controls (*teal* ●) and the fully inhibited controls in the presence of 10 μM of AL-11 (■). The *solid lines* represent the best fits by using linear regression with correlation coefficients of 0.9997 (●) and 0.855 (■), respectively. The data from the 17 h of incubation time were used for screen analysis. DMSO, dimethyl sulfoxide. Color images available online at www.liebertpub.com/adt

significant compound color interference, the impact turned out to be marginal, as illustrated in *Figure 2a*. The small increase in absorbance from the first to the last plates represents a delay between addition and reading, and this time was longer for the later plates. Data analysis showed that the substrate conversion was optimal at 17 h incubation time as the signal increased linearly with time over the investigated period, and this time point corresponded to less than 50% substrate conversion[41,42] and a signal well within the linear range of the microplate reader (*Fig. 2b*). Furthermore, both the signal from the uninhibited enzymatic reaction and the background values in fully inhibited wells (16 control wells each per plate) remained constant in all assay plates, demonstrating suitable stability of the enzyme, substrate, and control inhibitor solutions (*Fig. 3a*). The distinction between the controls was significant throughout the screening campaign, with calculated Z′ factors for individual plates ranging from 0.85 to 0.91 (*Fig. 3b*), and plate edge effects were largely absent (*Supplementary Fig. S1*).

The impact of the tested compounds is summarized in the form of a scatter plot in *Figure 3c*. A hit limit of 25.3% was calculated based on the average plus three standard deviations of the observed inhibitory response for all library compounds, resulting in a hit list of 165 compounds (1.6% hit rate). A selection of the most potent hits, for which the apparent inhibition in the primary screen was above 60%, was pursued in concentration-response experiments for confirmation purposes. Out of these 23 compounds, 16 confirmed concentration-dependent activity in the screening assay with an IC_{50} value around 10 μM or below (*Table 2* and *Fig. 4*).

One compound (1) originating from the Prestwick library of known drugs demonstrated sub-μM activity. The drug is known as Verteporfin and acts as a photosensitizer in the treatment of abnormal blood vessel formation in the eye. Based on the porphyrin motif, we suspect it could act as a chelator of the catalytically important Zn^{2+} ion in IRAP, but this remains to be demonstrated. Three additional drugs, chloroxine, merbromin, and vatalanib, were also at the top of the confirmed hit list with low μM inhibitory activity on IRAP. However, as can be seen from *Table 2*, several of these drugs regularly appear as hits in our internal screening campaigns, a measure referred to as the promiscuity index. It is well known that some compounds appear as pan-assay interfering compounds (PAINS), and several of these are drugs.[43–45] The frequent appearance of these in hit lists is also related to their application at significantly higher concentrations than what is required for therapeutic efficacy. Here, we were mainly interested in the identification of novel inhibitors with potential for selective inhibition of IRAP and thus used the promiscuity index to down-prioritize nonselective compounds with potentially unwanted mechanisms. Besides historical in-house data, these investigations also included PubChem BioAssay[46] and ChEMBL[47] (*Table 2*).

The hit compound solutions were analyzed for purity and the

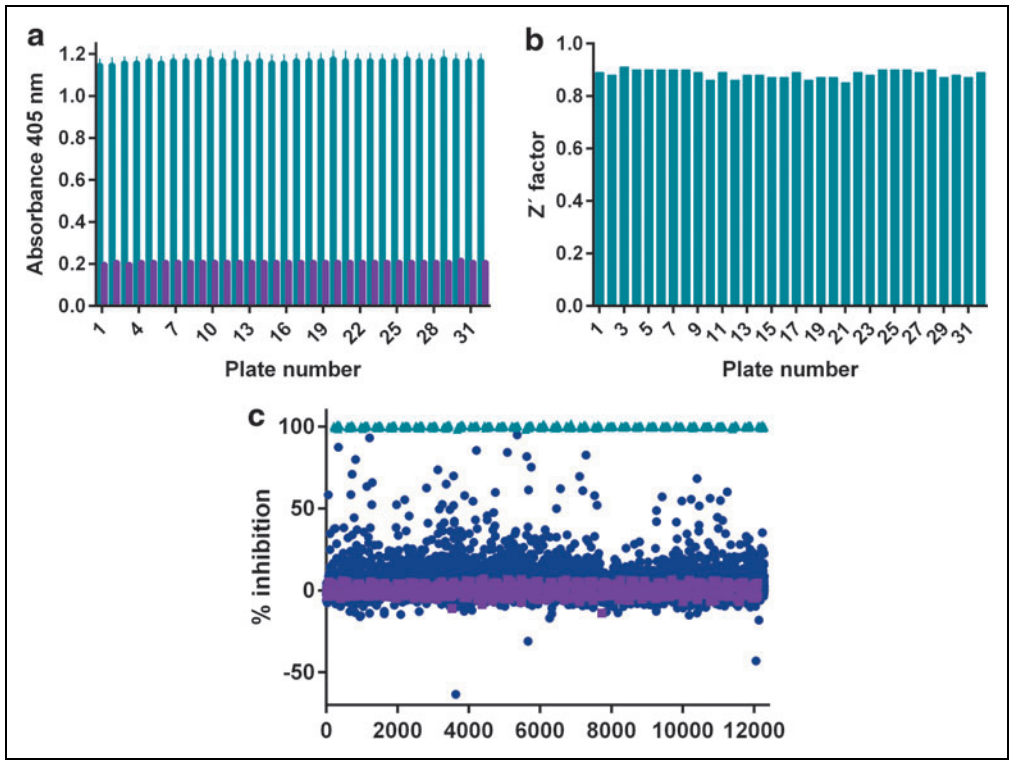

Fig. 3. Screen performance and hit identification. **(a)** Illustration of the average absorbance signal for the uninhibited controls (*teal bars*) and fully inhibited controls (*purple bars*) in the presence of 10 μM of AL-11. Data are shown as the average and standard error of mean (SEM) for the controls on each individual plate. **(b)** Illustration of the Z′ factor (*teal bars*) calculated based on the controls of each individual plate. **(c)** Scatter plot illustrating normalized screen data, where 0% corresponds to uninhibited IRAP in the presence of DMSO only (■), and 100% corresponds to fully inhibited IRAP in the presence of 10 μM of AL-11 (▲). The responses of the library compounds at a concentration of 10 μM are shown as *blue circles*. The screening experiment was performed in the presence of 1 mM of the L-Leu-*p*-NA substrate and CHO cell membranes from 25,000 cells in each well of the 384-well plates. SEM, standard error of mean. Color images available online at www.liebertpub.com/adt

Table 2. Summary Data for Top Hits in the IRAP Screening Campaign

Cmpd	Cmpd ID	Inhibition (%) at 10 μM	Correct mass[a]	Purity (%)[b]	IC_{50} (μM)[c]	Promiscuity[d]	No. of appearances ChEMBL or PubChem BioAssay	No. of analogs[e]
1	Verteporfin	93	Yes	95	0.29	3 (17)	0[f]	1/1/1
2		82	Yes	97	1.3 ± 0.3 (5)	1 (20)	0	39/6/1
3		68	Yes	58	2.0	1 (20)	0	20/9/1
4	Merbromin	80	n.a.	n.a.	2.2	9 (15)	>50	2/1/1
5		83	Yes	85	2.9	1 (16)	0	378/12/1
6		84	Yes	98	3.0 ± 0.3 (3)	2 (20)	0	46/10/2
7		75	Yes	100	3.1	1 (20)	0	24/8/3
8		70	Yes	100	3.5 (partial)	5 (14)	31	1/1/1
9		85	Yes	89	3.8	6 (15)	16	4/1/1
10		62	Yes	95	5.7 (partial)	1 (16)	0	111/15/1
11		70	Yes	97	5.8	1 (16)	0	12/2/1
12	Vatalanib	71	Yes	100	6.7	1 (16)	>50	1/1/1
13		62	Yes	99	6.7	1 (17)	0	213/29/4
14		60	Yes	78	10	3 (20)	0	16/1/1
15		61	Yes	84	11	2 (16)	0	385/29/2
16		60	Yes	98	11	1 (21)	0	91/21/4
17	Topotecan	66	Yes	75	27	5 (17)	>50	10/3/1
18		61	Yes	98	45 ± 34 (3)	2 (20)	0	20/6/3
19	Chloroxine	87	Yes	100	>72	2 (18)	>50	7/5/2
20		95	Yes	99	No (3)	1 (20)	0	220/16/2
21		74	No	99	No	6 (15)	0	11/8/1
22		65	Yes	6	No	1 (15)	0	2/1/1
23	Clioquinol	63	Yes	98	No	2 (17)	>50	5/4/2

Membrane preparations forming CHO cells were used as the IRAP activity source.

[a]Correct m/z ratio by LC-MS (ESI+).

[b]Purity according to LC-UV at 305 ± 90 and 254 nm.

[c]Numbers within brackets represent the number of test occasions on the screen batch solutions. Additional replicates were done on resynthesized compounds (see page 189, paragraph 1).

[d]Numbers represent the amount of times the compounds have appeared as hits in internal screens. Numbers within brackets represent the number of screens of which the compounds have been included as a part.

[e]Analog searches were based on the in-house cheminformatics program Beehive by using similarity searches with a Tanimoto coefficient >0.7. The numbers refer to available analogs in-house/tested in screen/actives above hit limit.

[f]Reported as part of training set for hepatotoxicity.

ESI, electrospray ionization; LC-MS, liquid chromatography-mass spectrometry.

appearance of the correct mass by using liquid chromatography and mass spectrometry-based detection (LC-MS) to associate the measured activities with the correct molecular structures. To prioritize among the hits, we also looked at the availability of structurally related analogs in our libraries that could be used to obtain fundamental structure-activity relationships (SAR). As shown in *Table 2*, these follow-up investigations identified six compounds denoted here as **2**, **5**, **7**, **11**, and **13**, all of which displayed (i) low μM apparent potency; (ii) the correct MS signal and a purity above 85% according to LC-

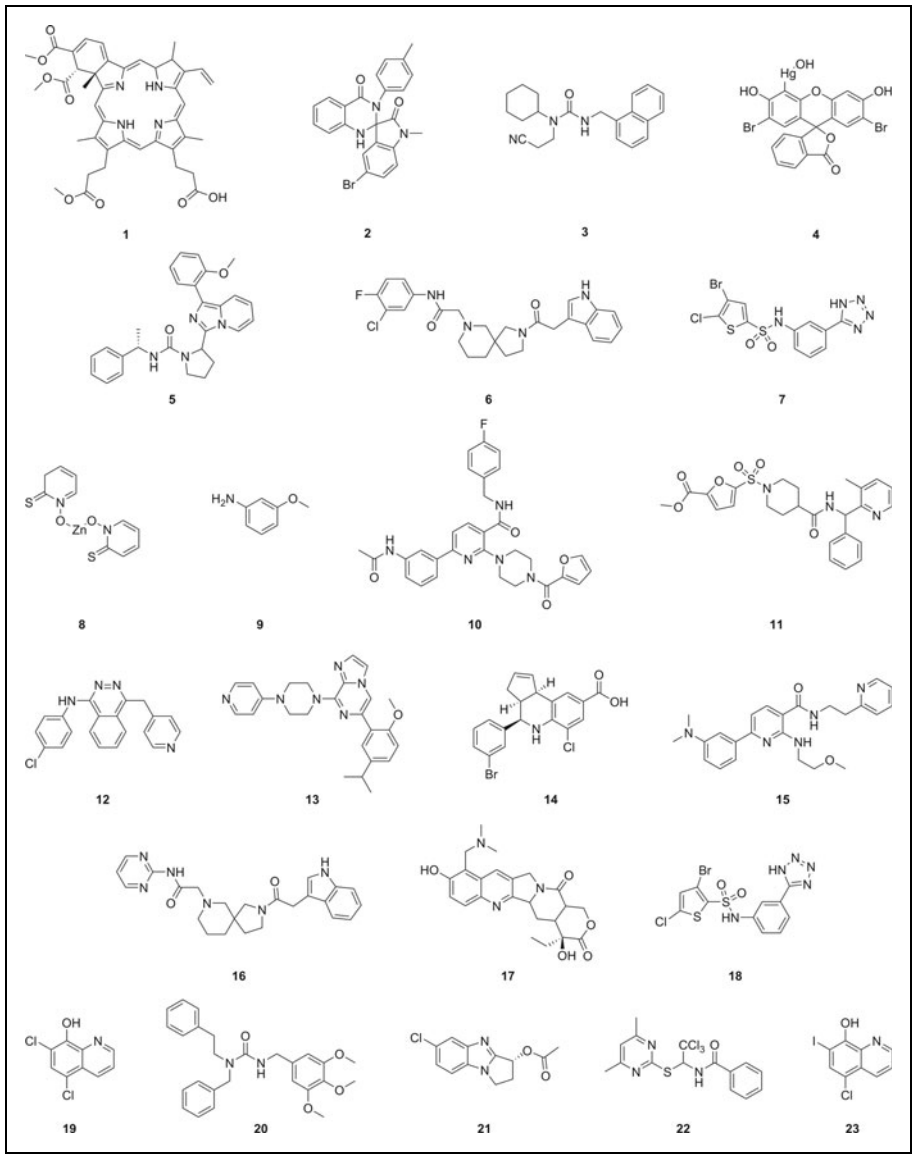

Fig. 4. Chemical structures of the top-ranked IRAP hits.

MS; (iii) no previous appearance as a hit in internal screening campaigns; (iv) a low incidence of reports in PubChem BioAssay and ChEMBL; and (v) relevant analogs available in-house. The three most potent representatives of this shortlist were initially considered for analog testing, resynthesis, and additional characterization to further validate them as starting points for development of small-molecule-based IRAP inhibitors. Synthetic protocols are already published for compounds **2**[35], **5**[48], and **7**.[36] In the library, compound **5** was epimeric at the C2 position of the pyrrolidine, but we chose to synthesize the compound with *S*-chirality since this corresponds to the natural amino acid L-proline. Evaluation of the IRAP inhibitory activity of this stereochemically pure isomer of **5** proved to be in the same order of magnitude as the hit compound (see Table 3). Hereafter, compound **5** with the defined stereochemistry at the C2 position will be referred to as **L-5**. The synthetic route to prepare **L-5** is illustrated in *Figure 5*.

Testing of the synthesized hits confirmed low μM inhibitory potency for all three compounds (*Fig. 6a*). Whereas the further SAR exploration for **7** has been published,[36] efforts are still ongoing to further expand the chemistry and SAR around **2** and **5** (to be published elsewhere). It should be noted that visual precipitation is observed at the highest test concentrations (>50 μM) for both compounds **2** and **L-5**, and especially for **2** this results in an elevated background absorbance and on occasion, the appearance of partial inhibition. In combination with the SAR exploration, we will also establish the inhibitory mechanism for these compounds, as this is required for calculation of K_i values. Meanwhile, the reported IC_{50} values must be treated as apparent estimates that are dependent on the current assay conditions.

Testing Reversibility and Activity in the Human Ortholog

To motivate further investments in these novel series of IRAP inhibitors, we pursued additional activity testing, broadly following a flowchart for characterization of reversible inhibitors.[49] Before this, we ensured the compounds did not interfere with the absorbance readout (*Supplementary Fig. S2*), also in agreement with the observation of inhibitory activity when running the assay based on the fluorogenic substrate L-Leu-AMC. We do, however, note a shift toward higher apparent potencies with the latter substrate (*Table 3*) for compounds **2** and **7**, prompting further investigations as to their inhibitory mechanisms.

With regards to the pharmacology of these compounds, we examined the Hill slopes of the concentration-response curves, which in all cases were close to unity, and the maximal inhibition obtained (*Fig. 6a*). Full inhibition was obtained for all these compounds, although a higher variability, sometimes resulting in partial inhibition, was observed for compound **2**

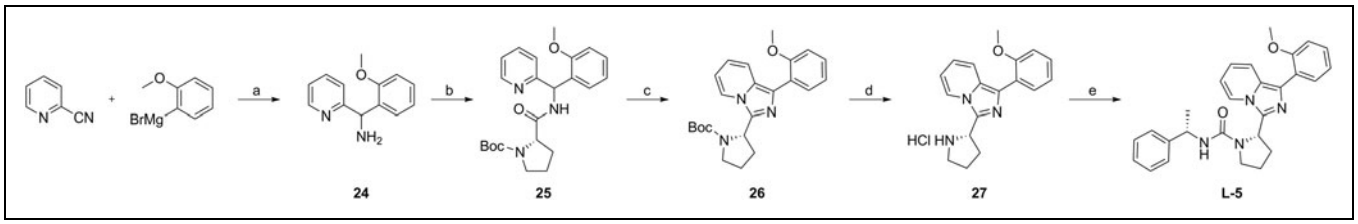

Fig. 5. Synthesis of compound **L-5**. Reagents and conditions: (a): (i) toluene, o°C; (ii) $NaBH_4$, 95%; (b) *N*-Boc-L-Pro, EDC*HCl, HOBt, TEA, and DCM, 94%; (c) $POCl_3$, pyridine, DCM, o°C, 84%; (d) HCl, dioxane, 99%; and (e) (*S*)-(-)-α-methylbenzyl isocyanate, TEA, MeCN, 71%.

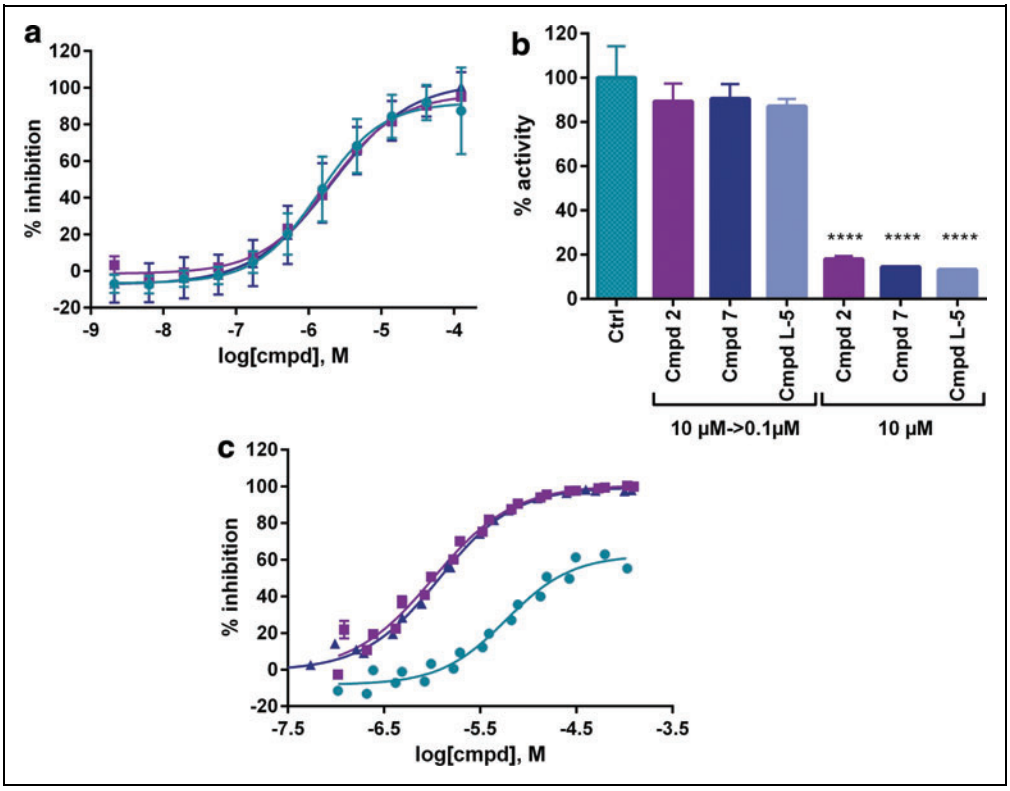

Fig. 6. Characterization of IRAP inhibition for resynthesized hits. **(a)** Normalized concentration-response curves for the inhibition of IRAP from CHO cells by cmpds **2** (●), **L-5** (■), and **7** (▲) in the presence of 1 mM of the L-Leu-*p*-NA substrate in 96-well plates. Data are presented as the average and standard deviation of results from multiple independent test occasions (cmpd **2** $n=14$; cmpd **L-5** $n=5$; cmpd **7** $n=12$). The *solid lines* represent best fits to a four-parameter sigmoidal curve in GraphPad Prism. **(b)** The reversibility of the inhibition was examined by means of rapid dilution experiments in which the CHO cell membrane preparations were exposed to 10 µM of hit compound either before or during the enzymatic assay. Reversibility was examined by a rapid 100-fold dilution such that the concentration during the assay became 0.1 µM. Data are shown as normalized values based on uninhibited controls and are given as the average and standard deviation from experiments done in triplicate for cmpds **2** (*purple*), **L-5** (*light blue*), and **7** (*dark blue*). The statistical significance was tested by using one-way ANOVA with no significant differences for the rapidly diluted solutions compared with controls, while the non-diluted samples were significantly inhibited ($p<0.0001$). **(c)** Normalized concentration-response curves for the inhibition of human IRAP. The symbols and assay conditions correspond to those in **(a)**, except that the CHO cell membrane preparations were replaced with membrane preparations from HEK293-F cells overexpressing human IRAP. Data are presented as the average and standard deviation of experiments done in triplicate on two independent test occasions. Color images available online at www.liebertpub.com/adt

(*Table 3* and *Fig. 6a*). This observation was concurrent with visual precipitation of the compound, demonstrating limited solubility. Although visual examination of the structures for potential reactive moieties did not suggest the involvement of covalent bond formation between IRAP and any of the inhibitors, rapid dilution experiments were also performed and proved that the enzymatic activity was quickly recovered on dilution, thus demonstrating that these inhibitors are rapidly reversible (*Fig. 6b*).

Concentration-response experiments in the presence of a reducing agent and a nonionic detergent were employed to investigate whether any of the compounds acted by means of unwanted protein inactivation through either cysteine oxidation or protein sequestering by aggregating compounds.[50–52] These control experiments showed that the inhibitory effect was largely independent of the presence of DTT or Triton X-100 (*Table 3*). The lack of evidence for these unwanted mechanisms is in agreement with the internal and external data on the absence of promiscuous appearances as hits in other screening campaigns. Furthermore, a search of the recently introduced public aggregator advisor database for

Table 3. Characterization of IRAP Inhibition Under Multiple Assay Conditions

No	L-Leu-p-NA IC_{50} (μM)	Hill slope	Maximal inhibition (%)	L-Leu-AMC IC_{50} (μM)	DTT[a] IC_{50} (μM)	T X-100[a] IC_{50} (μM)	hIRAP[b] IC_{50} (μM)
2	1.8 ± 0.95 (20)	0.99 ± 0.17	96 ± 7	6.9 ± 1.6[c]	1.6 ± 0.3[c]	3.7 ± 0.5	6.1 ± 1.0[c]
L-5	1.9 ± 0.26 (10)	0.99 ± 0.096	96 ± 2	3.2 ± 0.7[c]	2.1 ± 0.2	2.7 ± 0.5	1.1 ± 0.1
7	2.5 ± 1.2 (22)	0.84 ± 0.074	99 ± 3	14 ± 2	2.7 ± 0.7	6.3 ± 0.9	1.1 ± 0.2

All data were obtained on resynthesized and fully characterized material. Data are provided from triplicate samples at a minimum of two independent test occasions. CHO cell membrane preparations were used as the IRAP activity source. Cmpd **2** was tested as a racemate.

[a]Assay performed using L-Leu-*p*-NA as substrate in the presence of DTT or Triton X-100.

[b]Membrane preparations from human IRAP overexpressed in HEK293-F cells were used as the IRAP activity source.

[c]Partial inhibition observed.

DTT, dithiothreitol; L-Leu-AMC, L-leucine-7-amido-4-methylcoumarin.

these hit compounds did not show any relation to known aggregators, although a general warning was given based on the relatively high cLogP's.[52] It should also be noted that the experiments performed in the presence of Triton X-100, that is, conditions under which IRAP is known to be solubilized from the membrane, demonstrate that compound binding to IRAP is independent of the membrane anchoring.

Although CHO cells are known to abundantly express IRAP, we wanted to assert that the compounds were also active on human IRAP. Using the basic logical alignment search tool (BLAST),[53] we could conclude that IRAP from Chinese hamster (UniProtKB: A0A061IK54) and IRAP from human (UniProtKB: Q9UIQ6) have a sequence identity of 88.5%. For this purpose, human IRAP was overexpressed in HEK293-F suspension cells followed by membrane preparations to allow testing of activity of the three compounds (**2**, **L-5**, and **7**). All compounds proved to be active with similar potencies when tested on human IRAP, although compound **2** demonstrated more pronounced partial inhibition and about a threefold shift toward lower potency (*Table 3* and *Fig. 6c*). Further investigations are needed to understand to what extent this results from the limited solubility, or whether there are additional underlying causes of this behavior. As already mentioned, additional synthesis is ongoing to explore the SAR of this compound series and naturally the focus is on improving compound solubility.

DISCUSSION

A thorough understanding of the role of pharmacological inhibition of IRAP under normal physiological as well as disease conditions requires selective and potent modulators with good pharmacokinetic properties, the effects of which can be examined in relevant animal models. We have contributed in this field by variations of Ang IV itself, driven by the beneficial pharmacological effects observed on central administration of this degradation product originating from angiotensin II.[2–8] Based on the finding in 2001 that a central target for this effect is the aminopeptidase IRAP,[13] with activity toward cyclic peptides such as vasopressin and oxytocin, we have also worked with metabolically stable variants thereof,[21–25] with a primary focus are primarily focus on the field of cognition impairment. However, despite the possibility to generate potent peptide-based inhibitors, the majority of these suffer from preclinical challenges when administered systemically, particularly with regards to the limited cell permeability and penetrance of the blood–brain barrier. Significant advancements were made with the identification of small-molecule-based inhibitors of IRAP that demonstrated promising effects in animal models of cognition when administered centrally.[30,31] However, pending the further development of these inhibitors into new variants that can be administered systemically, there is a need to work broadly on additional molecular scaffolds.

We were interested in the identification of additional starting points by means of a small-molecule library screen. This was accomplished by using screen formatted variants of a well-published absorbance assay based on the dipeptide analog L-Leu-*p*-NA and membrane preparations from CHO cells as a natural rich source of IRAP activity. Given that small-molecule libraries are known to include colored compounds, we were concerned that the screen result would be significantly impacted by these compounds and in a worst case scenario that some inhibitors would be missed. However, this risk could be mitigated by running the screen in a semi-kinetic mode that included measurements of the absorbance at 405 nm of all library compounds. None of the compounds showed an absorbance above 20% of that measured as a consequence of substrate processing, and given that the hit limit was at ~25% we could conclude that no potent compounds were missed.

The screening campaign was successfully completed with excellent statistics and yielded 23 hits with an apparent inhibition above 60%. The majority of these confirmed activity in concentration-response experiments, resulting in the identification of several known drugs that interfered with IRAP activity. However, as the scope in this study was to identify new starting points that can be further developed into selective modulators of IRAP, we have not characterized these further. It is also worthwhile noting that many other biological activities are reported for a majority of these.

Instead, our primary focus was on those compounds that had not been previously active in our screening campaigns and that had no hitherto reported biological activities. Three compounds with low μM potency were of particular interest and were hence resynthesized, fully characterized, and examined for structure-activity relationships. Such efforts on compound **7** have been reported elsewhere,[36] whereas extended studies are presently ongoing for compounds **2** and **5**. Here, we have described a thorough characterization of these hit compounds with regards to their activity in an orthogonal assay based on a coumarin-based substrate and under different assay conditions to exclude commonly encountered artifacts due to compound aggregation and redox activities.[50–52] All compounds remain active under all tested conditions, including also the testing of activity on the human ortholog. Based on these findings, future studies will explore these compounds further, including not only structure-activity-based relationships but also further examinations of their mechanism of action through structural-based studies.

ACKNOWLEDGMENTS

H.A., M.O., K.S., A.J.J., and T.L. acknowledge Karolinska Institutet, SciLifeLab, and the Swedish Research Council (Vetenskapsrådet), which funds Chemical Biology Consortium Sweden. M.H. and M.L acknowledge the Kjell and Märta Beijer Foundation, King Gustav V's and Queen Victoria's Freemason Foundation, and Uppsala University for financial support.

DISCLOSURE STATEMENT

No competing financial interests exist.

REFERENCES

1. Prince M, Wimo A, Guerchet M, *et al.*: *World Alzheimer Report 2015, The Global Impact of Dementia, an Analysis of Prevalence, Incidence, Cost and Trends.* Alzheimer's Disease International, London, United Kingdom, 2015.
2. Braszko J, Kupryszewski G, Witczuk B, Wiśniewski K: Angiotensin II-(3–8)-hexapeptide affects motor activity, performance of passive avoidance and a conditioned avoidance response in rats. *Neuroscience* 1988;27:777–783.
3. Wright JW, Miller-Wing AV, Shaffer MJ, *et al.*: Angiotensin II(3–8) (ANG IV) hippocampal binding: Potential role in the facilitation of memory. *Brain Res Bull* 1993;32:497–502.
4. Wright JW, Clemens JA, Panetta JA, *et al.*: Effects of LY231617 and angiotensin IV on ischemia-induced deficits in circular water maze and passive avoidance performance in rats. *Brain Res* 1996;717:1–11.
5. Wright JW, Stubley L, Pederson ES, *et al.*: Contributions of the brain angiotensin IV-AT4 receptor subtype system to spatial learning. *J Neurosci* 1999;19:3952–3961.
6. Lee J, Albiston AL, Allen AM, *et al.*: Effect of I.C.V. injection of AT4 receptor ligands, NLE1-angiotensin IV and LVV-hemorphin 7, on spatial learning in rats. *Neuroscience* 2004;124:341–349.
7. Braszko JJ, Wielgat P, Walesiuk A: Effect of D(3) dopamine receptors blockade on the cognitive effects of angiotensin IV in rats. *Neuropeptides* 2008;42:301–309.
8. De Bundel D, Smolders I, Yang R, *et al.*: Angiotensin IV and LVV-haemorphin 7 enhance spatial working memory in rats: Effects on hippocampal glucose levels and blood flow. *Neurobiol Learn Mem* 2009;92:19–26.
9. Miller-Wing AV, Hanesworth JM, Sardinia MF, *et al.*: Central angiotensin IV binding sites: Distribution and specificity in guinea pig brain. *J Pharmacol Exp Ther* 1993;266:1718–1726.
10. Roberts KA, Krebs LT, Kramár EA, *et al.*: Autoradiographic identification of brain angiotensin IV binding sites and differential c-Fos expression following intracerebroventricular injection of angiotensin II and IV in rats. *Brain Res* 1995;682:13–21.
11. Moeller I, Chai SY, Oldfield BJ, *et al.*: Localization of angiotensin IV binding sites to motor and sensory neurons in the sheep spinal cord and hindbrain. *Brain Res* 1995;701:301–306.
12. Moeller I, Paxinos G, Mendelsohn FA, *et al.*: Distribution of AT4 receptors in the *Macaca fascicularis* brain. *Brain Res* 1996;712:307–324.
13. Albiston AL, McDowall SG, Matsacos D, *et al.*: Evidence that the angiotensin IV (AT(4)) receptor is the enzyme insulin-regulated aminopeptidase. *J Biol Chem* 2001;276:48623–48626.
14. Matsumoto H, Rogi T, Yamashiro K, *et al.*: Characterization of a recombinant soluble form of human placental leucine aminopeptidase/oxytocinase expressed in Chinese hamster ovary cells. *Eur J Biochem* 2000;267:46–52.
15. Wallis MG, Lankford MF, Keller SR: Vasopressin is a physiological substrate for the insulin-regulated aminopeptidase IRAP. *Am J Physiol Endocrinol Metab* 2007;293:E1092–E1102.
16. Saveanu L, Van Endert P: The role of insulin-regulated aminopeptidase in MHC class I antigen presentation. *Front Immunol* 2012;3:1–13.
17. Waters SB, D'Auria M, Martin SS, *et al.*: The amino terminus of insulin-responsive aminopeptidase causes Glut4 translocation in 3T3-L1 adipocytes. *J Biol Chem* 1997;272:23323–23327.
18. Lukaszuk A, Demaegdt H, Feytens D, *et al.*: The replacement of His(4) in angiotensin IV by conformationally constrained residues provides highly potent and selective analogues. *J Med Chem* 2009;52:5612–5618.
19. Lukaszuk A, Demaegdt H, Szemenyei E, *et al.*: Beta-homo-amino acid scan of angiotensin IV. *J Med Chem* 2008;51:2291–2296.
20. Nikolaou A, Eynde I, Van Den Tourwé D, *et al.*: [3H]IVDE77, a novel radioligand with high affinity and selectivity for the insulin-regulated aminopeptidase. *Eur J Pharmacol* 2013;702:93–102.
21. Axén A, Lindeberg G, Demaegdt H, *et al.*: Cyclic insulin-regulated aminopeptidase (IRAP)/AT4 receptor ligands. *J Pept Sci* 2006;12:705–713.
22. Axén A, Andersson H, Lindeberg G, *et al.*: Small potent ligands to the insulin-regulated aminopeptidase (IRAP)/AT(4) receptor. *J Pept Sci* 2007;13:434–444.
23. Andersson H, Demaegdt H, Vauquelin G, *et al.*: Ligands to the (IRAP)/AT4 receptor encompassing a 4-hydroxydiphenylmethane scaffold replacing Tyr2. *Bioorganic Med Chem* 2008;16:6924–6935.
24. Andersson H, Demaegdt H, Vauquelin G, *et al.*: Disulfide cyclized tripeptide analogues of angiotensin IV as potent and selective inhibitors of insulin-regulated aminopeptidase (IRAP). *J Med Chem* 2010;53:8059–8071.
25. Andersson H, Demaegdt H, Johnsson A, *et al.*: Potent macrocyclic inhibitors of insulin-regulated aminopeptidase (IRAP) by olefin ring-closing metathesis. *J Med Chem* 2011;54:3779–3792.
26. Diwakarla S, Nylander E, Gronbladh A, *et al.*: Binding to and inhibition of insulin-regulated aminopeptidase (IRAP) by macrocyclic disulfides enhances spine density. *Mol Pharmacol* 2016;89:413–424.

27. Zervoudi E, Saridakis E, Birtley JR, *et al.*: Rationally designed inhibitor targeting antigen-trimming aminopeptidases enhances antigen presentation and cytotoxic T-cell responses. *Proc Natl Acad Sci U S A* 2013;110:19890–19895.
28. Papakyriakou A, Zervoudi E, Theodorakis E, A, *et al.*: Novel selective inhibitors of aminopeptidases that generate antigenic peptides. *Bioorganic Med Chem Lett* 2013;23:4832–4836.
29. Papakyriakou A, Zervoudi E, Tsoukalidou S, *et al.*: 3,4-diaminobenzoic acid derivatives as inhibitors of the oxytocinase subfamily of M1 aminopeptidases with immune-regulating properties. *J Med Chem* 2015;58:1524–1543.
30. Albiston AL, Morton CJ, Ng HL, *et al.*: Identification and characterization of a new cognitive enhancer based on inhibition of insulin-regulated aminopeptidase. *FASEB J* 2008;22:4209–4217.
31. Mountford S, J, Albiston A, L, Charman W, N, *et al.*: Synthesis, structure-activity relationships and brain uptake of a novel series of benzopyran inhibitors of insulin-regulated aminopeptidase. *J Med Chem* 2014;57:1368–1377.
32. Demaegdt H, Vanderheyden P, De Backer J-P, *et al.*: Endogenous cystinyl aminopeptidase in Chinese hamster ovary cells: Characterization by [125I]Ang IV binding and catalytic activity. *Biochem Pharmacol* 2004;68:885–892.
33. Demaegdt H, Lukaszuk A, De Buyser E, *et al.*: Selective labeling of IRAP by the tritiated AT4 receptor ligand [3H]Angiotensin IV and its stable analog [3H]AL-11. *Mol Cell Endocrinol* 2009;311:77–86.
34. Zhang J-H, Chung TD, Oldenburg KR: A simple statistical parameter for use in evaluation and validation of high throughput screening assays. *J Biomol Screen* 1999;4:67–73.
35. Engen K, Sävmarker J, Rosenström U, *et al.*: Microwave heated flow synthesis of spiro-oxindole dihydroquinazolinone based IRAP inhibitors. *Org Process Res Dev* 2014;18:1582–1588.
36. Borhade SR, Rosenström U, Sävmarker J, *et al.*: Inhibition of insulin-regulated aminopeptidase (IRAP) by arylsulfonamides. *ChemistryOpen* 2014;3:256–263.
37. Laustsen PG, Vang S, Kristensen T: Mutational analysis of the active site of human insulin-regulated aminopeptidase. *Eur J Biochem* 2001;268:98–104.
38. Lew RA, Mustafa T, Ye S, *et al.*: Angiotensin AT4 ligands are potent, competitive inhibitors of insulin regulated aminopeptidase (IRAP). *J Neurochem* 2004;86:344–350.
39. Demaegdt H, Lenaerts P, J, Swales J, *et al.*: Angiotensin AT4 receptor ligand interaction with cystinyl aminopeptidase and aminopeptidase N: [125I]Angiotensin IV only binds to the cystinyl aminopeptidase apo-enzyme. *Eur J Pharmacol* 2006;546:19–27.
40. Lundholt BK, Scudder KM, Pagliaro L: A simple technique for reducing edge effect in cell-based assays. *J Biomol Screen* 2003;8:566–570.
41. Wu G, Yuan Y, Hodge CN: Determining appropriate substrate conversion for enzymatic assays in high-throughput screening. *J Biomol Screen* 2003;8:694–700.
42. Tholander F: Improved inhibitor screening experiments by comparative analysis of simulated enzyme progress curves. *PLoS One* 2012;7:e46764.
43. Baell JB, Holloway GA: New substructure filters for removal of pan assay interference compounds (PAINS) from screening libraries and for their exclusion in bioassays. *J Med Chem* 2010;53:2719–2740.
44. Baell JB: Observations on screening-based research and some concerning trends in the literature. *Future Med Chem* 2010;2:1529–1546.
45. Baell J, Walters MA: Chemistry: Chemical con artists foil drug discovery. *Nature* 2014;513:481–483.
46. Wang Y, Xiao J, Suzek T, O, *et al.*: PubChem's BioAssay database. *Nucleic Acids Res* 2012;40:D400–D412.
47. Bento AP, Gaulton A, Hersey A, *et al.*: The ChEMBL bioactivity database: An update. *Nucleic Acids Res* 2014;42:D1083–D1090.
48. Ward TJ, Crossley R, Slater MJ: Biofocus Discovery Ltd.: Imidazopyridine derivatives as BSR-3 antagonists. WO2005080390, February 16, 2005.
49. Copeland RA: Lead optimization and structure-activity relationships for reversible inhibitors. In: *Evaluation of Enzyme Inhibitors in Drug Discovery: A Guide for Medicinal Chemists and Pharmacologists*. pp. 169–201. John Wiley & Sons, Inc., Hoboken, New Jersey.
50. Thorne N, Auld DS, Inglese J: Apparent activity in high-throughput screening: Origins of compound-dependent assay interference. *Curr Opin Chem Biol* 2010;14:315–324.
51. Acker MG, Auld DS: Considerations for the design and reporting of enzyme assays in high-throughput screening applications. *Perspect Sci* 2014;1:56–73.
52. Irwin JJ, Duan D, Torosyan H, *et al.*: An aggregation advisor for ligand discovery. *J Med Chem* 2015;58:7076–7087.
53. Altschul SF, Gish W, Miller W, Myers EW, Lipman DJ: Basic local alignment search tool. *J Mol Biol* 1990;215:403–410.

Address correspondence to:
Thomas Lundbäck, PhD
Chemical Biology Consortium Sweden
Science for Life Laboratory Stockholm
Division of Translational Medicine and Chemical Biology
Department of Medical Biochemistry and Biophysics
Karolinska Institutet
Tomtebodavägen 23A
Solna 171 65
Sweden

E-mail: thomas.lundback@ki.se

Mats Larhed, PhD
Science for Life Laboratory Uppsala
Division of Organic Pharmaceutical Chemistry
Department of Medicinal Chemistry
Uppsala University
P.O. Box 574
Uppsala 751 23
Sweden

E-mail: mats.larhed@orgfarm.uu.se

Abbreviations Used

Ang IV = angiotensin IV
CBCS = Chemical Biology Consortium Sweden
CHO = Chinese hamster ovary
Cmpd = compound
DCM = dichloromethane
DMSO = dimethyl sulfoxide
DTT = dithiothreitol
EDC = *N*-(3-dimethylaminopropyl)-*N'*-ethylcarbodiimide
ERAP = endoplasmic reticulum aminopeptidase
ESI = electrospray ionization
HOBt = 1-hydroxybenzotriazole hydrate
HPLC = high-performance liquid chromatography
HRMS = high-resolution mass spectra
IRAP = insulin-regulated aminopeptidase
K_i = inhibitory constant
LC-MS = liquid chromatography-mass spectrometry
L-Leu-AMC = L-leucine-7-amido-4-methylcoumarin
L-Leu-*p*-NA = L-leucine-*para*-nitroanilide
MS = mass spectrometry
PAINS = pan-assay interfering compounds
PBS = phosphate-buffered saline
PMSF = phenylmethanesulfonyl fluoride
SAR = structure-activity relationships
SEM = standard error of mean
TEA = triethylamine
THF = tetrahydrofuran